THE JOURNAL OF BIOLOGICAL CHEMISTRY VOL. 292, NO. 15, pp. 6255–6268, April 14, 2017

Mechanistic insights into the allosteric regulation of bacterial ADP-glucose pyrophosphorylases

Received for publication, December 21, 2016, and in revised form, February 17, 2017 Published, JBC Papers in Press, February 21, 2017, DOI 10.1074/jbc.M116.773408

Natalia Comino[‡1], **Javier O. Cifuente**[‡1], **Alberto Marina**[‡], **Ane Orrantia**[‡], **Ander Eguskiza**[‡], **and Marcelo E. Guerin**[‡§¶‖2]

From the [‡]*Structural Biology Unit, CIC bioGUNE, Bizkaia Technology Park, 48160 Derio, Spain,* [§]*Unidad de Biofísica, Centro Mixto Consejo Superior de Investigaciones Científicas-Universidad del País Vasco/Euskal Herriko Unibertsitatea (CSIC,UPV/EHU), Barrio Sarriena s/n, Leioa, 48940 Bizkaia, Spain,* [¶]*Departamento de Bioquímica, Universidad del País Vasco, Leioa, 48940 Bizkaia, Spain, and* [‖]*IKERBASQUE, Basque Foundation for Science, 48013 Bilbao, Spain*

Edited by Gerald W. Hart

ADP-glucose pyrophosphorylase (AGPase) controls bacterial glycogen and plant starch biosynthetic pathways, the most common carbon storage polysaccharides in nature. AGPase activity is allosterically regulated by a series of metabolites in the energetic flux within the cell. Very recently, we reported the first crystal structures of the paradigmatic AGPase from *Escherichia coli* (*Ec*AGPase) in complex with its preferred physiological negative and positive allosteric regulators, adenosine 5′-monophosphate (AMP) and fructose 1,6-bisphosphate (FBP), respectively. However, understanding the molecular mechanism by which AMP and FBP allosterically modulates *Ec*AGPase enzymatic activity still remains enigmatic. Here we found that single point mutations of key residues in the AMP-binding site decrease its inhibitory effect but also clearly abolish the overall AMP-mediated stabilization effect in wild-type *Ec*AGPase. Single point mutations of key residues for FBP binding did not revert the AMP-mediated stabilization. Strikingly, an *Ec*AGPase-R130A mutant displayed a dramatic increase in activity when compared with wild-type *Ec*AGPase, and this increase correlated with a significant increment of glycogen content *in vivo*. The crystal structure of *Ec*AGPase-R130A revealed unprecedented conformational changes in structural elements involved in the allosteric signal transmission. Altogether, we propose a model in which the positive and negative energy reporters regulate AGPase catalytic activity via intra- and interprotomer cross-talk, with a "sensory motif" and two loops, RL1 and RL2, flanking the ATP-binding site playing a significant role. The information reported herein provides exciting possibilities for industrial/biotechnological applications.

Glycogen and starch are the major carbon and energy reserve polysaccharides in nature. Glycogen is a very large branched glucose homopolymer containing ~90% α-(1→4)-glucoside linkages and 10% α-(1→6)-glucoside linkages (1, 2). Glycogen is found in archaea, heterotrophic bacteria, fungi, and higher eukaryotes, localizing as discrete cytoplasmic granules of <50 nm (3). Eukaryotes utilize UDP-glucose as the activated nucleotide donor for glycogen biosynthesis, whereas archaebacteria and bacteria have selected ADP-Glc, defining two different pathways with distinct regulatory mechanisms and rate-controlling steps (2, 4–7). In bacteria, the basic biosynthetic pathway of glycogen involves the action of three enzymes: ADP-glucose pyrophosphorylase (AGPase),[3] glycogen synthase (GS), and branching enzyme (BE; Refs. 6 and 8). AGPase catalyzes the biosynthesis of the nucleotide sugar donor, ADP-Glc (Ref. 9; Fig. 1). The second step is catalyzed by GS, which transfers a glucose residue to the hydroxyl group at position 4 of a glucose residue located at the non-reducing end of glycogen to form an α-(1→4)-glucoside linkage (10–13). It is worth noting that in fungi and higher eukaryotes glycogenin-linked maltooligosaccharides provide the initial glycogen primer for further elongation by GS (14–16). In contrast, bacterial glycogen *de novo* synthesis seems not to require the presence of α-(1→4)-linked glucans, with GS catalyzing the initiation and elongation reactions (17–19). The third step is catalyzed by BE, which forms the α-(1→6) branch points in glycogen (8). Specifically, BE cleavage α-(1→4)-glucosidic linkage in glycogen, yielding a non-reducing end oligosaccharide chain, with subsequent attachment of the oligosaccharide to the α-(1→6) position of the polymer (20, 21). Glycogen degradation is carried out by glycogen phosphorylase (GP; Ref. 22), which functions as a depolymerizing enzyme, and the debranching enzyme that catalyzes the removal of α-(1→6)-linked ramifications (23).

The main regulatory step in the bacterial glycogen biosynthetic pathway is carried out by AGPase (9, 24, 25). AGPase catalyzes a condensation reaction between ATP and α-D-glucose-1-phosphate (G1P) to produce ADP-Glc and pyrophosphate (Refs. 9 and 26; Fig. 1). Specifically, the oxygen on the phosphate group of G1P acts as a nucleophile attacking the

This work was supported by European Commission Contract HEALTH-F3-2011-260872, Spanish Ministry of Economy and Competitiveness Contract BIO2013-49022-C2–2-R, and the Basque Government (to M. E. G.). The authors declare that they have no conflicts of interest with the contents of this article.

This article contains supplemental Table S1 and Figs. S1 and S2.

The atomic coordinates and structure factors (code 5MNI) have been deposited in the Protein Data Bank (http://wwpdb.org/).

[1] Both authors contributed equally to this work.

[2] To whom correspondence should be addressed: Structural Biology Unit, CIC bioGUNE, Bizkaia Technology Park, 48160 Derio, Spain. Tel.: 34-944-061-309; E-mail: mrcguerin@cicbiogune.es.

[3] The abbreviations used are: AGPase, ADP-glucose pyrophosphorylase; *Ec*AGPase, AGPase from *E. coli*; GS, glycogen synthase; BE, branching enzyme; GP, glycogen phosphorylase; G1P, α-D-glucose-1-phosphate; GT-A-like, glycosyltransferase-A like domain; LβH, left-handed β-helix domain; FBP, fructose 1,6-bisphosphate; SM, sensory motif; F6P, fructose 6-phosphate; LDH, lactate dehydrogenase; SUC, sucrose.

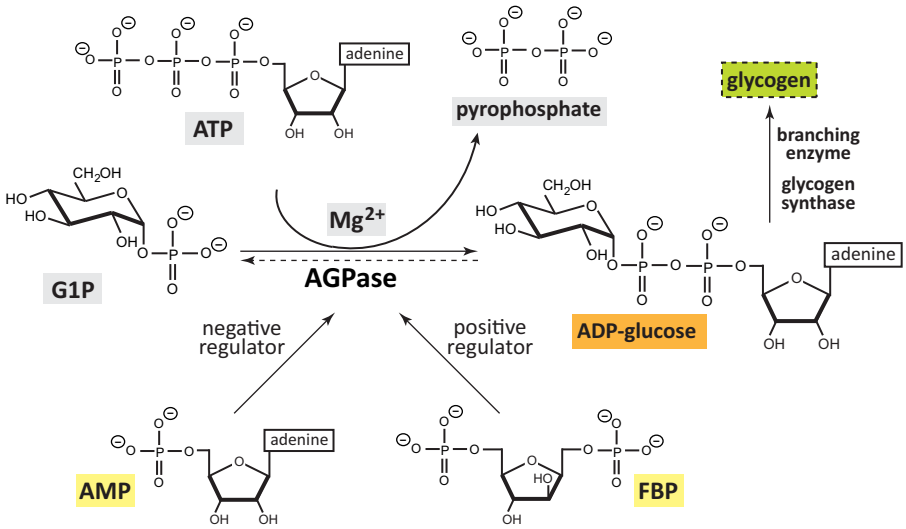

Figure 1. Chemical reaction catalyzed by *Ec*AGPase. *Ec*AGPase catalyzes the main regulatory step in bacterial glycogen. *Ec*AGPase catalyzes the reaction between ATP and G1P in the presence of a divalent metal cation, Mg^{2+}, to form ADP-Glc and pyrophosphate (26). The enzymatic reaction is reversible *in vitro*. However, the hydrolysis of inorganic pyrophosphate by inorganic pyrophosphatase results in an irreversible reaction *in vivo* in the direction of ADP-Glc biosynthesis (9). ADP-Glc biosynthesis and hydrolysis directions are shown as a *full* and *dotted lines*, respectively. The two major positive (FBP) and negative (AMP) allosteric regulators are shown. The biosynthesis of bacterial glycogen in *E. coli*, essentially involve the action of two other consecutive enzymes, the glycogen synthase and branching enzyme.

α-PO_4 group of the nucleoside triphosphate, leading to the liberation of pyrophosphate (PP_i; 27). The reaction is held in the presence of the divalent metal cation Mg^{2+}, which minimizes the charge repulsion between phosphate groups, inducing/favoring nucleophile activation (28). In addition, two positively charged residues polarize these groups, increasing the nucleophilic nature of the oxygen attacking the phosphor atom (29, 30). AGPase follows a sequential ordered bi-bi mechanism with ATP binding first followed by G1P and ordered release of pyrophosphate and ADP-Glc (31). The hydrolysis of pyrophosphate by the action of inorganic pyrophosphatases results in a global irreversible and energetically expensive reaction *in vivo* (32, 33). As a consequence, evolution led AGPase to acquire an exquisite allosteric regulation mechanism to control its enzymatic activity by essential metabolites in the energetic flux within the cell (31, 34, 35). AGPase activators are metabolites that reflect signals of high carbon and energy content of a particular bacteria or tissue, whereas inhibitors of the enzyme indicate low metabolic energy levels (9, 36). Based on the specific positive or negative allosteric regulators, AGPases have been classified into nine different classes (9, 34).

Bacterial AGPases are encoded by a single gene, giving rise to a native homotetrameric protein ($\alpha4$) with a molecular mass of ~200 kDa (9). In the case of the paradigmatic bacterial AGPase from *Escherichia coli* (*Ec*AGPase), each protomer is encoded by a single gene (*glgC*) located inside an operon together with the genes that code for GS (*glgA*), GP (*glgP*), BE (*glgB*), and phosphoglucomutase (*pgm*; Refs. 37 and 38). To date, two crystal structures of bacterial AGPases have been reported, that of *Ec*AGPase (Fig. 2*A*; Ref. 26) and *Agrobacterium tumefaciens* (*At*AGPase; Ref. 39). Each protomer comprises two domains, the N-terminal glycosyltransferase-A like domain (GT-A-like), where the active site is located, and the C-terminal left-handed β-helix domain (LβH; Refs. 26 and 39–42). *Ec*AGPase dimerizes by an end-to-end stacking of two β-helix domains, whereas the tetramer assembly is mainly mediated by the interaction of GT-A-like domains. The resulting architecture allows the protomers to communicate with each other, from which cooperativity emerges (26, 39, 43). Very recently, the crystal structures of the paradigmatic *Ec*AGPase were solved in complex with its preferred physiological positive and negative allosteric regulators, fructose 1,6-bisphosphate (FBP) and adenosine 5′-monophosphate (AMP), respectively (Fig. 2*A*; Ref. 26), defining four common allosteric clefts between the GT-A-like and LβH domains of neighboring protomers in which both allosteric modulators binds to partially overlapping sites. This structural configuration of the *Ec*AGPase regulatory site accounts for the fact that sensitivity to inhibition by AMP is modulated by the concentration of the activator FBP (24, 44). Specifically, each allosteric cleft is communicated with the corresponding active site of the same protomer through a region defined as the sensory motif (SM), a complex structural element constituted by the nucleotide-binding loop NBL, including a G-rich motif involved in ATP binding and a segment rich in short secondary structure elements (26). Altogether we proposed a model in which the binding of the positive and negative energy reporters regulate *Ec*AGPase catalytic activity through the SM and two critical regulatory loops, RL1 and RL2, flanking the active binding site via intra-protomer interactions and inter-protomer cross-talk (26).

Here we carefully explore the consequences of single point mutations in the allosteric cleft of *Ec*AGPase in key residues involved in FBP and AMP binding, looking for changes in the allosteric properties, stabilization, and their impact in enzymatic activity. We explore how those mutations impact in the yield of glycogen in the physiological environment of the host. Finally, in combination with the crystal structure of an *Ec*AGPase single point mutant, we provide important mechanistic insights into the regulatory mechanism by which *Ec*AGPase modulates catalysis at the molecular level.

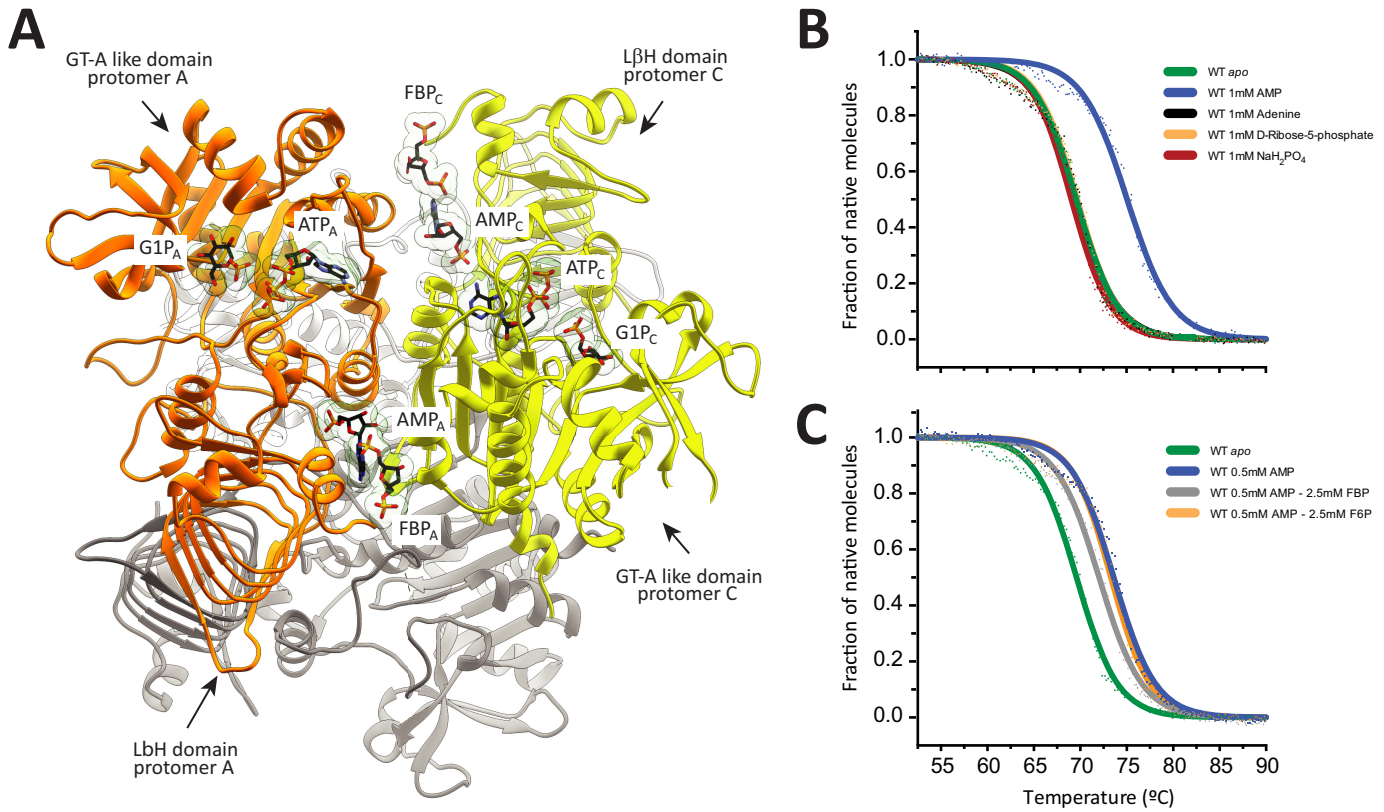

Figure 2. Dissecting the structural determinants of *Ec*AGPase regulation. *A*, ribbon representation of the overall homotetrameric structure of *Ec*AGPase showing the location of the active and regulatory sites. AMP, FBP, ATP, and G1P molecules are shown in two protomers from different dimers of the *Ec*AGPase homotetramer. Protomers A and C are shown in *orange* and *yellow*, respectively. The location of the ATP-binding site in *Ec*AGPase was determined by structural superposition with the crystal structure of *N*-acetylglucosamine-1-phosphate uridyltransferase in complex with ATP (PDB code 4K6R) and that of AGPase from *S. tuberosum* in complex with ATP and ADPG (PDB code 1YP3). The G1P-binding site in *Ec*AGPase was determined taking into account the location of the glucose moiety of sucrose in the *Ec*AGPase-AMP-SUC complex (5L6V). *B*, thermal unfolding for the unliganded form of *Ec*AGPase (*green*) and the *Ec*AGPase-AMP (*blue*), *Ec*AGPase-Adenine (*black*), *Ec*AGPase-5RP (*yellow*), and *Ec*AGPase-PO_4 (*red*) complexes. *C*, thermal unfolding for the unliganded form of *Ec*AGPase (*green*) and the *Ec*AGPase-AMP (*blue*), *Ec*AGPase-AMP-FBP (gray), and *Ec*AGPase-AMP-F6P complexes.

Results and discussion

Dissecting the structural determinants of EcAGPase allosteric regulation

The crystal structures of the *Ec*AGPase-AMP-SUC (PDB code 5L6V) and *Ec*AGPase-FBP (PDB code 5L6S) complexes revealed that the allosteric regulators AMP and FBP bind to a common regulatory cleft defined by the GT-A-like and LβH domains of neighboring protomers (26). AMP is deeply buried into the cleft, defined by (i) the N-terminal β2-β3 hairpin (residues 46–52), α5, and the connecting loop α2-α3 (residues 37–42) and (ii) the C-terminal α15 (residues 419–425) and the connecting loops β28-β29 (residues 384–388) and β25-β26 (residues 367–371; Figs. 2*A* and 3). In addition, AMP makes strong contacts with neighbor protomers of the homotetramer, leading to the stabilization of the quaternary structure of the enzyme. Specifically, the *Ec*AGPase-AMP complex was ~4.6 °C more stable than the unliganded form of the enzyme (26). In contrast, FBP is located in a more solvent-exposed environment, mainly comprised by the last C-terminal residues of the enzyme (residues 420–431; Ref. 26). Interestingly, the addition of FBP to the *Ec*AGPase-AMP complex triggered a clear reduction in the apparent melting temperatures (T_m) values, indicating that FBP is able to compete with AMP and to modify the structural arrangement of the *Ec*AGPase-AMP complex, leading to a less stable structure (26, 45). Supporting this notion, (i) the structural comparison of the *Ec*AGPase-AMP-SUC and *Ec*AGPase-FBP crystal structures revealed that the AMP- and FBP-binding sites partially overlap, and (ii) sensitivity to inhibition by AMP is modulated by the concentration of the activator FBP (34).

To further advance the understanding of the molecular mechanism of *Ec*AGPase allosteric regulation, we studied the contribution of a series of chemical derivatives of AMP and FBP to the stabilization of the enzyme. To this end, the ellipticity of *Ec*AGPase in the presence of AMP, orthophosphate, D-ribose 5-phosphate, adenine, FBP, and fructose 6-phosphate (F6P) was monitored at 222 nm as a function of temperature. Upon the addition of AMP, the T_m value of EcAGPase increased from 65.6 °C to 73.6 °C (Fig. 2*B*). In contrast, the presence of orthophosphate, D-ribose 5-phosphate, and adenine did not significantly affect the T_m value of *Ec*AGPase, with 69.0 °C, 69.7 °C, and 69.5 °C values, respectively (Fig. 2*B*). These experimental observations correlated well with the structural configuration of the AMP allosteric site as visualized in the *Ec*AGPase-AMP-SUC crystal structure (Fig. 3; Ref. 26). Specifically, the α-PO_4 of AMP localizes in a pocket composed of Arg-40, His-46, Arg-52, and Arg-386 of the same protomer, with no evident interactions with adjacent protomers of the

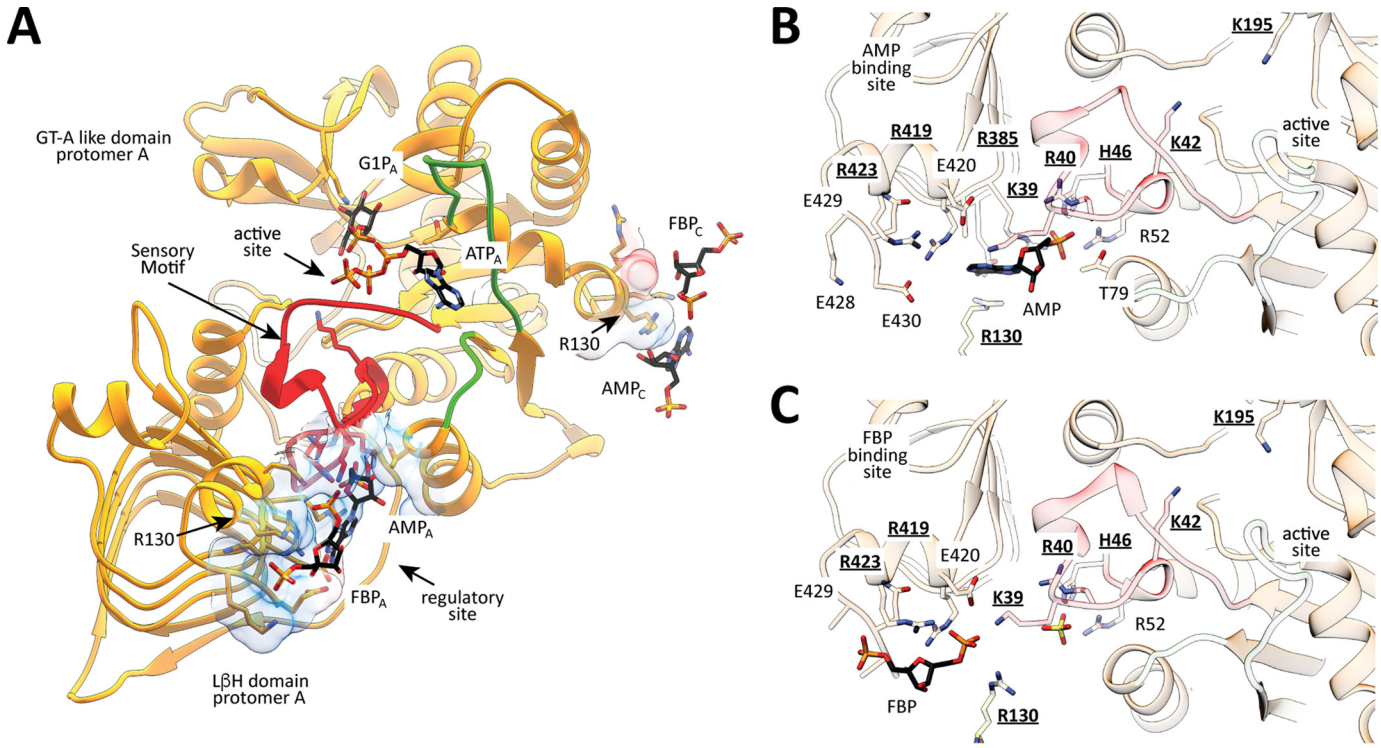

Figure 3. Localization of residues in the active and regulatory sites in *Ec*AGPase. *A*, *Ec*AGPase protomer showing the GT-A-like and LβH domains. *B*, close view of the AMP regulatory site showing the location of key residues involved in AMP binding and its communication with the active site of *Ec*AGPase. Selected/mutated residues are *underlined*. *C*, close view of the FBP regulatory site showing the location of key residues involved in FBP binding and its communication with the active site of *Ec*AGPase. Selected/mutated residues are *underlined*.

homotetramer (Fig. 3*B*). Similarly, the D-ribose moiety of D-ribose 5-phosphate provides two additional interactions with Lys-39 and Thr-79, also located in the same protomer. Interestingly, the *Ec*AGPase-AMP-SUC crystal structure revealed that the adenine heterocycle is stabilized by a strong stacking interaction with Arg-130 (α7) from the GT-A-like domain of a neighboring protomer (Figs. 2*A* and 3, *A* and *B*). However, the nucleobase alone did not provide any measurable stabilization effect.

Different moieties of the AMP chemical scaffold have been studied regarding their modulatory effects on *Ec*AGPase activity. Orthophosphate was characterized as a weak inhibitor of *Ec*AGPase, requiring a much higher concentration to achieve similar inhibitory levels than AMP (24). Most of the AGPase crystal structures reported to date revealed the presence of either orthophosphate or sulfate anions located in the corresponding binding pocket of the α-PO_4 moiety of AMP in the regulatory site of *Ec*AGPase (26, 39, 46). Interestingly, structural evidence also revealed the presence of (i) orthophosphate in the active site of *Ec*AGPase (26) and (ii) sulfate, a phosphate mimic, in the active site of *Solanum tuberosum* AGPase (*St*AGPase), with the ATP substrate in a non-catalytically active conformation (PDB code 1YP3; Ref. 46). This structural information might suggest a competitive inhibitory effect of these anions with the *Ec*AGPase substrates at high concentrations; however, an intra-protomeric inhibitory effect cannot be discarded. Finally, the presence of D-ribose 5-phosphate or adenine did not alter the activity of *Ec*AGPase (47, 48). Altogether, these experimental observations indicate that the complete AMP scaffold is required for the stabilization of the enzyme, strongly supporting the notion that AMP inhibitory properties are inherently linked to the inter-protomer cross-talk in the negative allosteric mechanism of *Ec*AGPase.

Finally, the addition of FBP to the *Ec*AGPase-AMP complex produced a clear reduction in the T_m value, whereas the presence of F6P did not significantly affect the T_m value of the *Ec*AGPase-AMP complex. Taking into consideration that F6P does not modulate *Ec*AGPase activity (34) together with its inability to alter *Ec*AGPase-AMP stability points toward the PO_4 group at position 1 of fructose as a key player in enhancing the enzymatic activity to modulate AMP inhibition and to reverse AMP stabilization effect (Figs. 2*B* and 3*C*).

Design of EcAGPase single point mutants in the regulatory cleft and active site

We carefully explored the consequences of single point mutations in the allosteric cleft of *Ec*AGPase in key residues involved in AMP and FBP binding, looking for changes in the allosteric properties, stabilization, and their impact in enzymatic activity (Fig. 3). Residues facing the allosteric cleft, Lys-39, Arg-40, His-46, Arg-130, Arg-386, Arg-419, and Arg-423, were selected and replaced by alanine. Residues Lys-39, Arg-40, His-46, and Arg-130 belong to the N-terminal GT-A-like domain, whereas Arg-386, Arg-419, and Arg-423 are located in the LβH domain (Figs. 2*A* and 3). Specifically, Lys-39, Arg-40, and His-46 are located in the SM motif, Arg-386 are in the β25-β26 loop of the LβH domain, and residues Arg-419 and Arg-423 are in the C-terminal α15 (26). The crystal structure of the *Ec*AGPase-AMP-SUC revealed that (i) the α-PO_4 group of the negative regulator AMP interacts with Arg-40, His-46, and

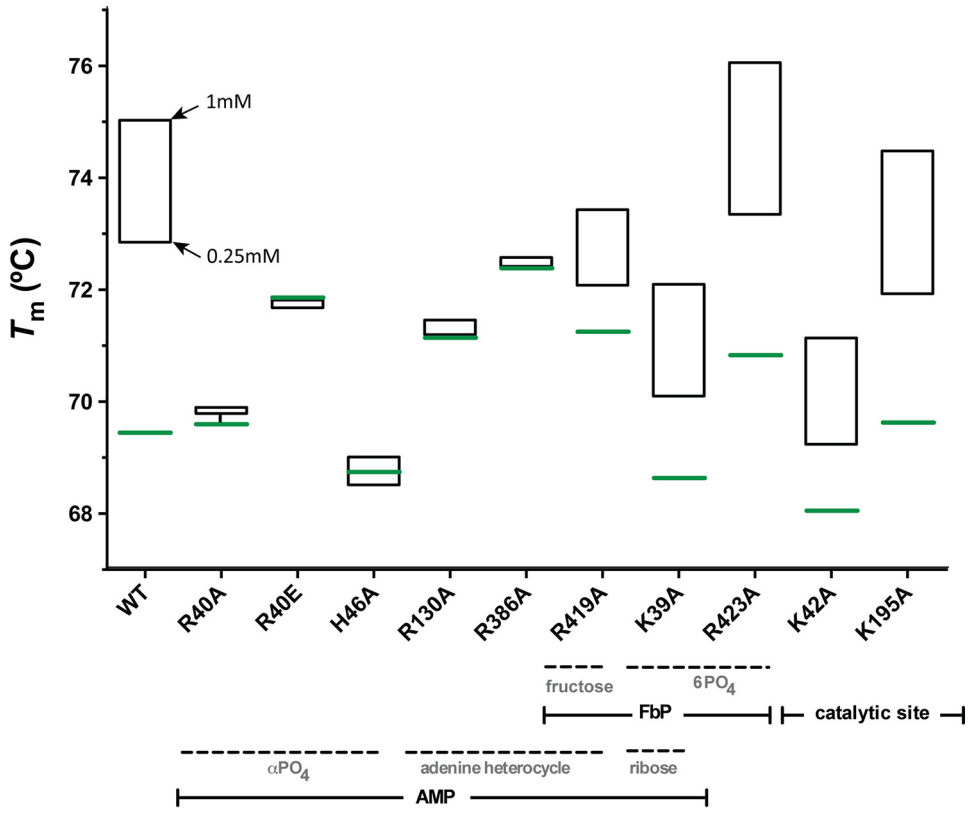

Figure 4. Thermal unfolding transitions of *Ec*AGPase and selected *Ec*AGPase variants in complex with AMP. Thermal unfolding transitions were recorded at 222 nm between 20 °C and 90 °C. T_m value for the apo state of *Ec*AGPase and selected *Ec*AGPase variants are shown in *green*. AMP concentrations are shown in *black*.

Arg-386, and (ii) the D-ribose moiety is at a van der Waals distance of Lys-39. In addition, the adenine heterocycle is stabilized by a strong stacking interaction with Arg-130 and additional van der Waals interactions with Arg-419 and Arg-386 (Fig. 3*B*; Ref. 26). Based on the *Ec*AGPase-FBP crystal structure, residues Lys-39, Arg-419, and Arg-423 of the same protomer interact with the PO_4 group at position 6 of FBP; meanwhile Arg-130 in the neighbor protomer appears at salt-bridge distance. It is worth noting that Lys-39 proved to be essential for the FBP-mediated enzymatic activation to take place (44).

Single point mutants of the predicted catalytic residues, Lys-42 and Lys-195, were constructed by replacing them by alanine (30, 49, 50). The predicted catalytic residue Lys-42 is located in a key region of the SM motif, at very close distance of several residues participating in both AMP and FBP regulators interactions, in the regulatory cleft. Moreover, the side chain of Lys-42 is in close contact with two aspartic residues, Asp-142 and Asp-276 (26, 39, 51, 52), which were suggested to participate in the interaction of the divalent metal cation Mg^{2+} during catalysis, as observed in other nucleotidyltransferases (28, 53). Finally, Lys-195 is located in the β12-β13 loop of the sugar-binding pocket, in the active site of the GT-A-like domain, far apart from the allosteric cleft. Lys-195 was proposed to interact with the β-PO_4 group of ADP-Glc (26, 46). It is worth noting that no *Ec*AGPase constructs encode additional amino acids when compared with the native enzyme. They were expressed and purified to apparent homogeneity following three main steps including anionic exchange, ammonium sulfate precipitation, and hydrophobic interaction criteria (see "Experimental procedures" for details).

Single point mutants localized in the regulatory cleft impact EcAGPase stabilization

The addition of AMP did not modify the T_m values of the *Ec*AGPase-R40A, *Ec*AGPase-R46A, *Ec*AGPase-R130A, and *Ec*AGPase-R386A mutants (Fig. 4), strongly supporting a role of these residues in AMP binding, as visualized in the crystal structure of the *Ec*AGPase-AMP-SUC complex (Figs. 3 and 4). In contrast, the addition of AMP to the *Ec*AGPase-K39A, *Ec*AGPase-R419A, and *Ec*AGPase-R423A mutants, which are involved in FBP recognition, according to the *Ec*AGPase-FBP crystal structure, triggered a clear increment in the T_m values as observed in the wild-type enzyme (26). As expected, the stabilization of *Ec*AGPase-K42A and *Ec*AGPase-K195A mutants, the predicted catalytic residues, was not affected by the addition of the negative regulator. Interestingly, the addition of FBP to the *Ec*AGPase-K39A and *Ec*AGPase-R419A was unable to revert the stabilization of the enzyme variants mediated by AMP. In contrast, some reversion was observed in *Ec*AGPase-R423A (Fig. 5; Ref. 26). As expected, *Ec*AGPase-K195A displays a similar behavior. However, the T_m value of the *Ec*AGPase-K42A mutant in the presence of AMP or AMP/FBP regulators remained equally stable. Because the side chain of Lys-42 is in close contact with two aspartic residues, Asp-142 and Asp-276 (26, 39, 51, 52), this phenomenon might reflect the communication between the allosteric and active sites.

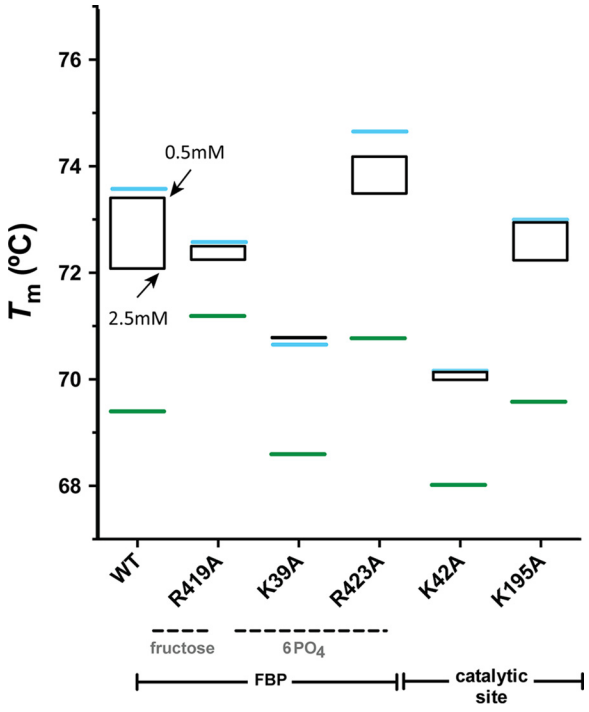

Figure 5. Thermal unfolding transitions of *Ec*AGPase and selected single point mutants in the presence of AMP and FBP. Thermal unfolding transitions were recorded at 222 nm between 20 °C and 90 °C. T_m value for the apo state of *Ec*AGPase and selected *Ec*AGPase variants are shown in *green*. The T_m values of *Ec*AGPase and selected *Ec*AGPase variants in complex with AMP at 1 mM are shown in *blue*. FBP concentrations are shown in *black*.

EcAGPase-R130A deregulates AMP-mediated inhibition of the enzymatic activity, inducing the overproduction of glycogen in vivo

To characterize the impact of the single point mutations on the allosteric properties of *Ec*AGPase, we measured their specific activities by the colorimetric end-point malachite green phosphate assay. *Ec*AGPase-R130A doubled the specific activity compared with the wild-type *Ec*AGPase in the absence of allosteric regulators (Fig. 6). As expected, wild-type *Ec*AGPase is highly activated by FBP, but in contrast, most mutants failed to reach similar levels of activity compared with the *Ec*AGPase-FBP active state (Fig. 6). Interestingly, *Ec*AGPase-R130A was the only mutant activated by FBP, consistent with the requirement of an intra-protomeric signaling for the activation of the enzyme. Nevertheless, its activity did not reach the same levels of the wild type, which could be attributable to the lack of additional mechanism to reach full activation, the interprotomeric cross-talk.

In the presence of AMP, *Ec*AGPase-R40A, *Ec*AGPase-R40E, and *Ec*AGPase-H46A mutants (the mutated residues interact with the AMP α-PO_4) along with the *Ec*AGPase-R130A and *Ec*AGPase-R386A mutants (the mutated residues interact with the adenine heterocycle and D-ribose moieties of AMP, respectively) displayed a similar behavior as that observed for the wild-type enzyme. Specifically, a partial inhibition was shown in all cases, pointing to a compensatory effect of the mutated residues. No inhibition was detected in the *Ec*AGPase-K39A and *Ec*AGPase-R419A mutants (the mutated residues interact with the D-ribose and adenine heterocycle moieties of AMP, respectively). The *Ec*AGPase-R423A displayed behavior similar to the wild-type enzyme, which is consistent with the lack of interactions between this residue and AMP. The effect of the negative regulator AMP was also addressed in the presence of FBP, as sensitivity to inhibition by AMP is modulated by the concentration of the activator FBP (Fig. 6; Refs. 24, 34, and 44). Strikingly, *Ec*AGPase-R130A displayed (i) a similar specific activity than in the presence of FBP and (ii) 7-fold higher than the wild-type enzyme in the presence of both AMP and FBP regulators, revealing a deregulation of the inactivation mediated by AMP for this mutant. Interestingly, the *Ec*AGPase-K39A and *Ec*AGPase-R419A mutants were unable to completely revert the slight activation induced by FBP in the presence of AMP, which is consistent with the results observed in the thermal unfolding transitions in the presence of both modulators (Fig. 5). As expected, *Ec*AGPase-K42A and *Ec*AGPase-K195A mutants, the predicted catalytic residues, were inactive in all conditions tested.

To study the impact of the single point mutations in the *in vivo* glycogen content of *E. coli*, the *E. coli* K-12 Δ*glgC* pTARA strain was transformed with pET22b-*Ec*AGPase or the corresponding mutants (see "Experimental procedures" for details). The cultures were synchronized, and aliquots were removed every hour before and after the induction for the determination of glycogen content. The growth curves of the different *Ec*AGPase mutants confirmed that they were in the exponential growth phase in all cases (Fig. 7*A*). After glycogen extraction, a standard anthrone assay was used for the detection of sugars (Fig. 7*B*). As a complementary approach, a less sensitive but more specific iodimetric method was also used to measure glycogen content (Fig. 7*C*). As expected, the *Ec*AGPase-K42A and *Ec*AGPase-K195A mutants carrying out the predicted catalytic residues were unable to accumulate glycogen. Strikingly, *Ec*AGPase-R130A mutant displayed an overproduction of glycogen *in vivo*, which correlates with the specific activities measured for this variant *in vitro*, supporting the notion of a hyperactive deregulated enzyme. Interestingly, *Ec*AGPase-R40E mutant displayed a glycogen content similar to that observed with *Ec*AGPase-R130A, although its specific activities did not show clear evidences of being a highly active enzyme. It is worth noting that *Ec*AGPase is mainly activated by FBP; however, it can be also activated by other glycolytic intermediates (34, 54). The change in the charge of *Ec*AGPase-R40E in the regulatory cleft might, therefore, modify the effect of other regulators *in vivo*, highlighting the complexity of the allosteric mechanism of this key enzyme.

The crystal structure of EcAGPase-R130A reveals unprecedented conformational changes in key structural elements involved in EcAGPase allosteric regulation

The crystal structure of *Ec*AGPase-R130A was solved in its unliganded form at 3.09 Å resolution (PDB code 5MNI; supplemental Table S1). *Ec*AGPase-R130A crystallized in space group $P\,2_1$ with eight molecules in the asymmetric unit, representing two homotetramers of the enzyme. When compared with the *Ec*AGPase-AMP-SUC and *Ec*AGPase-FBP complexes (26), the crystal structure of *Ec*AGPase-R130A revealed significant conformational changes. First, the two dimers of the homotetramer

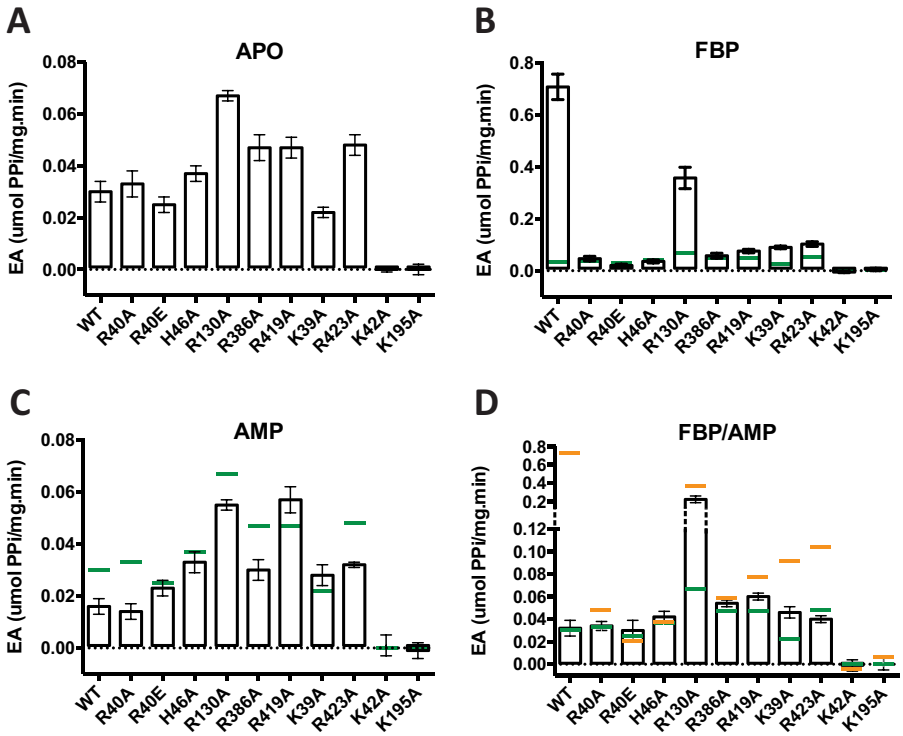

Figure 6. Activity measurements of *Ec*AGPase and selected *Ec*AGPase variants. The enzymatic activity of *Ec*AGPase and selected *Ec*AGPase variants was measured in the absence of allosteric regulators (*A*), in the presence of FBP (*B*), in the presence of AMP (*C*), and in the presence of both positive and negative regulators FBP and AMP (see "Experimental procedures" for details). The activity values for *Ec*AGPase (*green*) and *Ec*AGPase-FBP (*orange*) are shown as *lines* as a reference.

were reoriented, strongly suggesting conformational flexibility of the quaternary structure of *Ec*AGPase (Fig. 8, *A* and *B*; supplemental Fig. S1). Moreover, conformational differences were also observed in key elements implicated in the proposed allosteric regulatory mechanism (26). Specifically, residues 26–41 of the SM motif displayed a new extended conformation, partially overlapping the α-PO_4- and D-ribose-binding sites of AMP, observed in the *Ec*AGPase-AMP-SUC structure (Fig. 8*C*; supplemental Fig. S1). The side chain of Arg-419 makes hydrogen-bonding interactions with the main chain carbonyl group of Leu-34 and the side chain of Asn-38. Interestingly, in the other seven protomers this region of the SM was found partially disordered. The *Ec*AGPase-AMP-SUC and *Ec*AGPase-FBP crystal structures revealed that both AMP- and FBP-binding sites partially overlap, pointing to an important role of dynamics and conformational changes of several structural elements located in the regulatory cleft in the signal transduction mechanism. The replacement of Arg-130 by alanine certainly affected the transduction of the negative regulatory signal to the active site, likely due to an interprotomer crosstalk mechanism, as suggested by the *Ec*AGPase-AMP-SUC crystal structure. However, the absence of Arg-130 might also modify the rearrangement/dynamics of other structural elements located in the regulatory site of *Ec*AGPase, most notably the SM motif, contributing to the activation/cooperativity of the enzyme.

Similarly, the RL1 loop, which is in close contact with the nucleotide-binding loop (NBL) (residues 26–33) including the GG*X*G*X*R consensus sequence involved in ATP binding, was also observed to adopt different structural arrangements. Interestingly, the replacement of the highly conserved Tyr-75 per alanine resulted in an inactive enzyme, suggesting a functional role for this residue in the modulation of the enzymatic activity, as reported for the Q74A mutant (45). Finally, RL2 could only be observed/partially modeled in a different conformation with respect to the *Ec*AGPase-AMP-SUC and *Ec*AGPase-FBP structures. Taken together, the new crystal structure of *Ec*AGPase-R130A provides evidence of conformational changes including local flexibility in key elements proposed to be involved in allosteric communication.

EcAGPase shares common sequence signatures for allosteric regulator binding with other enterobacterial AGPases

Multiple primary structure alignment among members of the Enterobacteriaceae family of AGPases revealed Lys-42 and Lys-195, the proposed catalytic residues, along with Arg-40, His-46, Arg-386, and Arg-130, residues involved in AMP binding, highly preserved (Fig. 9). Some experimental data indicated that the C-terminal region of *Ec*AGPase is involved in the recognition of the positive regulator and allosteric activation mechanism of the enzyme (54). Specifically, (i) the ^{419}R*X*ML-RKL*XX*KQER^{431} sequence and (ii) the key residue Lys-39, which were observed to interact with the positive regulator FBP in the *Ec*AGPase-FBP complex, are strictly conserved among enterobacterial AGPases known to use FBP as a positive regulator (26, 34, 54). Based on primary structure alignment, enterobacteria families that have not been studied in terms of their allosteric activators and conserve this C-terminal region are predicted to also be regulated by FBP (*Shigella flexneri*, *Shigella boydii*, *Salmonella choleraesuis*, *Escherichia fergusonii*; Fig. 9).

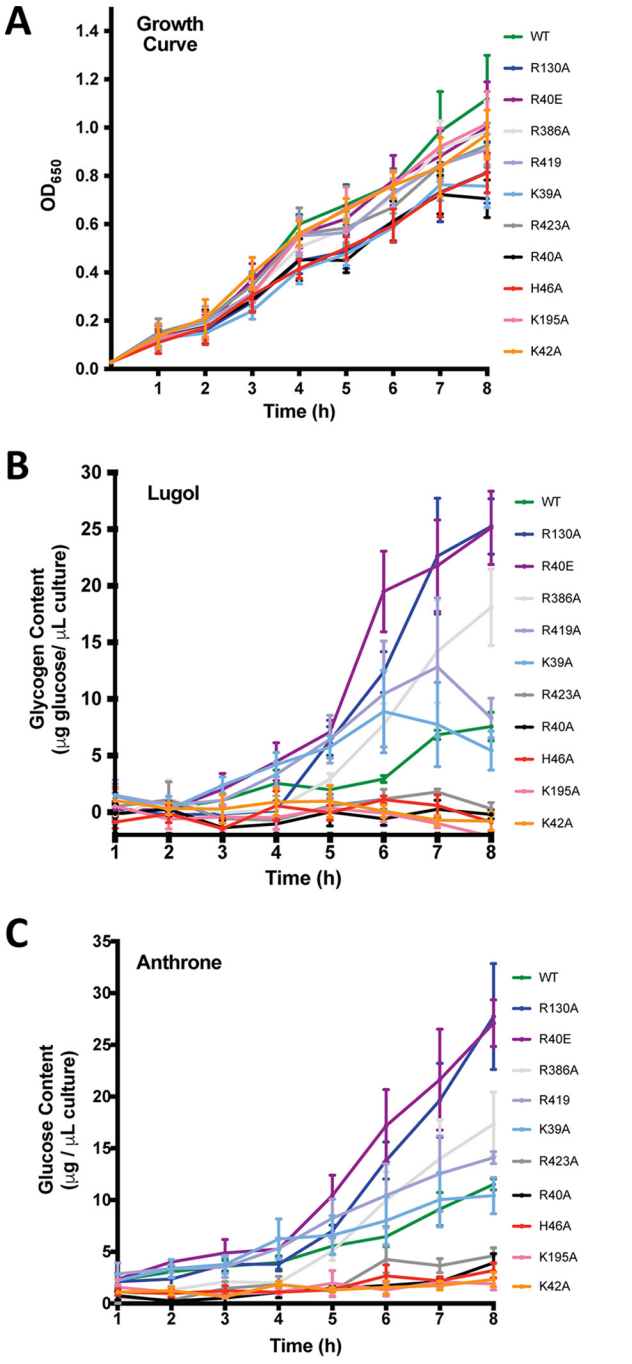

Figure 7. Glycogen content *in vivo*. *A*, growth curve. *B*, glycogen content by using Lugol method (71). *C*, glycogen content by using anthrone method (72, 82).

Interestingly, some enterobacterial AGPases not regulated by FBP (34, 54) displayed clear discrepancies in the C-terminal region (*Serratia marcescens*, *Serratia liquefaciens*, *Hafnia alvei*), strongly suggesting that other enterobacteria AGPases lacking this region might have a different positive regulatory mechanism (*Yersinia pestis*, *Pantoea vagans*, *Erwinia* sp., *Pectobacterium atrosepticum*, *Dickeya dadantii*, *Proteus vulgaris*; Figs. 9 and 10).

Cell energy metabolism is inherently linked to the evolution of organisms; thus, enterobacterial glycogen synthesis ought to be studied in this context. Based on our observations, AGPase seems to follow the same phylogenetic history of the Enterobacteriaceae family, as described in the Pathosystems Resource Integration Center (55). In this regard, the conserved use of FBP as positive allosteric regulator in *Ec*AGPase seems to be a trait acquired by a subgroup of enterobacterial AGPases sharing the C-terminal ^{419}R*X*MLRKL*XX*KQER^{431} sequence (supplemental Fig. S2).

Conclusion

Allosteric proteins are biological control systems and are considered one of the most elaborate products of molecular evolution (56). A convergence evolution in allosteric molecular mechanisms and symmetry in quaternary architectures have been observed in unrelated proteins. Early studies pointed out homotropic cooperative effect characteristics compatible with Monod-Wyman-Changeaux model of *Ec*AGPase (24). Interestingly, other enzymes of the central energy metabolism display similarities at structural and regulatory levels to *Ec*AGPase, like pyruvate kinase, lactate dehydrogenase (LDH), and glycerol kinase (57, 58, 59). These enzymes are homotetramers with D2 symmetry that binds FBP as allosteric effector in some organisms. As for *Ec*AGPase, in all these enzymes, the allosteric phenomenon was proposed to occur after the Monod-Wyman-Changeaux model (60), where the symmetry of the tetrameric system must be preserved, and the catalytic properties are explained by conformational displacement between the so called "tense" low-activity/affinity state (T-state) and a "relaxed" high-activity/affinity state (R-state) in a concerted fashion among protomers. These structurally distinct conformational states had been structurally observed bound to modulators (61, 62). It is worth noting that although pyruvate kinase and LDH use FBP as positive allosteric modulators, glycerol kinase is inhibited by this metabolite. Altogether, the experimental data suggest that the crystal structure of *Ec*AGPase-AMP-SUC very likely represents the conformational state of the T-state. The allosteric charge cleft is conserved among AGPases providing the place of interaction of different negatively charged modulators. The geometry of the ligands and their specific interaction with the charged side chains might result in differential tensions across the structure, which leads ultimately to local rearrangements and global conformational changes. In this regard, parallelism can be drawn for *Ec*AGPase-R130A compared with LDH, where reduction in positive charge in the tetramer interface deregulates a bacterial LDH and stabilizes its tetrameric structure (63).

Finally, the transformation of plants with *E. coli* allosteric mutants on the *glgC* gene significantly increased (i) the rate of starch synthesis in tubers of transgenic potato (64) and (ii) starch content (65, 66). Therefore, the information reported herein provides exciting possibilities for industrial/biotechnological applications.

Experimental procedures

Materials

The pET22b-*Ec*AGPase^{K39A}, pET22b-*Ec*AGPase^{R40A}, pET22b-*Ec*AGPase^{R40E}, pET22b-*Ec*AGPase^{K42A}, pET22b-*Ec*AGPase^{H46A}, pET22b-*Ec*AGPase^{R130A}, pET22b-*Ec*AGPase^{K195A}, pET22b-*Ec*AGPase^{R386A}, pET22b-*Ec*AGPase^{R419A}, and pET22b-

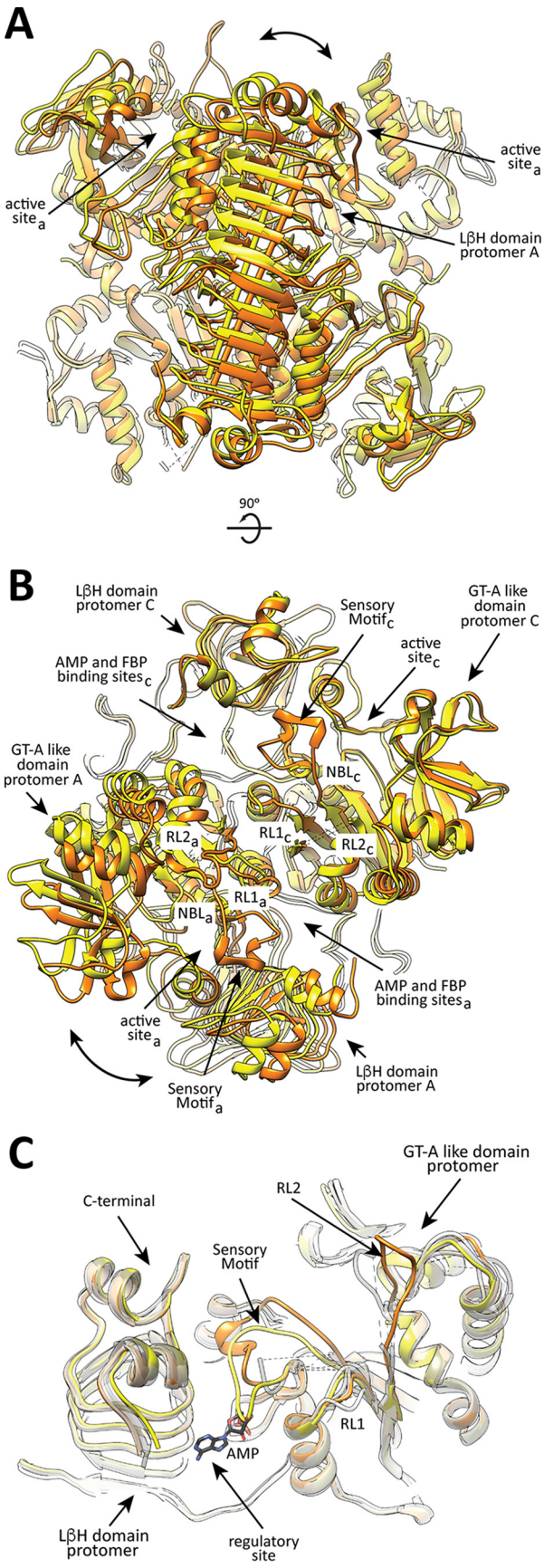

Figure 8. The crystal structure of *Ec*AGPase-R130A. *A* and *B*, two views of the structural superposition between the *Ec*AGPase-R130A (*yellow*) and *Ec*AGPase-FBP (*orange*) tetramers, based on the alignment of LβH domains pairs (*arrow*). The relative rotation of both domains is shown (*curved arrow*). *C*, *Ec*AGPase-R130A structure (protomer D: *yellow*) centered at the sensory motif, superimposed with an *Ec*AGPase-AMP-SUC protomer (*orange*), revealing the prominent conformational changes leading the SM motif to partially occupy the AMP-binding site. The other *Ec*AGPase-R130A protomers of the asymmetric unit appear superposed in *gray scale*, showing variability in the RL1, RL2 regions and the G-rich loop.

*Ec*AGPase^{R423A} plasmids carrying out the *Ec*AGPase mutants were synthesized/sequenced by ATG:biosynthetics (Merzhausen, Germany) using the pET22b-*Ec*AGPase clone as template (see "Materials" for EcAGPase cloning) and further expressed and purified to apparent homogeneity as described for the recombinant *Ec*AGPase enzyme.

EcAGPase cloning, expression, and purification

The full-length *glgC* gene from *E. coli* BL21 was amplified by standard PCR using oligonucleotide primers *glgC*_NdeI_Fwd (5′-GGGAATTCCATATGGTTAGTT-3′) and *glgC*_XhoI_Rev (5′-CCGCTCGAGTCATCGCTCCTG-3), Phusion DNA Polymerase (New England BioLabs), and purified genomic DNA as the template. The PCR fragment was digested with NdeI and XhoI and purified by agarose gel electrophoresis. The fragment was ligated to the expression vector pET22b (Novagen) using T4 DNA ligase, generating pET22b-*Ec*AGPase. The recombinant *Ec*AGPase has no additional amino acids when compared with the native enzyme. *E. coli* BL21(DE3) cells transformed with pET22b-*Ec*AGPase or the corresponding mutants were grown in 2000 ml of LB medium (5 g of yeast extract, 10 g of peptone Tryptone, 10 g of NaCl) supplemented with 100 μg/ml carbenicillin at 37 °C. When the culture reached an A_{600} of 0.8, *Ec*AGPase expression was induced by the addition of 1 mM isopropyl β-thiogalactopyranoside and further incubated at 18 °C for 20 h. Cells were harvested by centrifugation at 5000 $\times$ *g* and resuspended in 40 ml of 50 mM Hepes, pH 8.0, 5 mM $MgCl_2$, 0.1 mM EDTA, 10% sucrose (w/v; solution A) containing protease inhibitors (Complete EDTA-free; Roche Applied Science) and 10 mg/liter of lysozyme (Sigma). Cells were then disrupted by sonication (24 cycles of 10 s each) and centrifuged for 20 min at 20,000 $\times$ *g*. The supernatant was dialyzed twice against solution A by using a 100,000-Da molecular mass cutoff dialysis membrane. The solution was then applied to a Q-Sepharose packed column (30 ml; GE Healthcare) equilibrated with solution A. Elution was performed with a linear 0–0.5 M NaCl gradient in 100 ml. Enzymatically active fractions were pooled and incubated with 1.2 M ammonium sulfate final concentration (solution B). The resultant suspension was centrifuged for 20 min at 32,000 $\times$ *g*, and the supernatant was applied into a Phenyl Shodex HIC PH-814 column equilibrated in solution B. The enzyme was eluted with a linear gradient of 100% solution B to 100% solution A in 50 ml. The protein was dialyzed against solution A with a 100-kDa molecular mass cutoff overnight and stored at −80 °C. All the mutants were purified following the same protocol.

Thermal unfolding

Thermal unfolding transitions were recorded on a J-815 CD spectropolarimeter (Jasco Corp., Tokio, Japan) equipped with a water-cooled Peltier unit. Measurements were carried out at

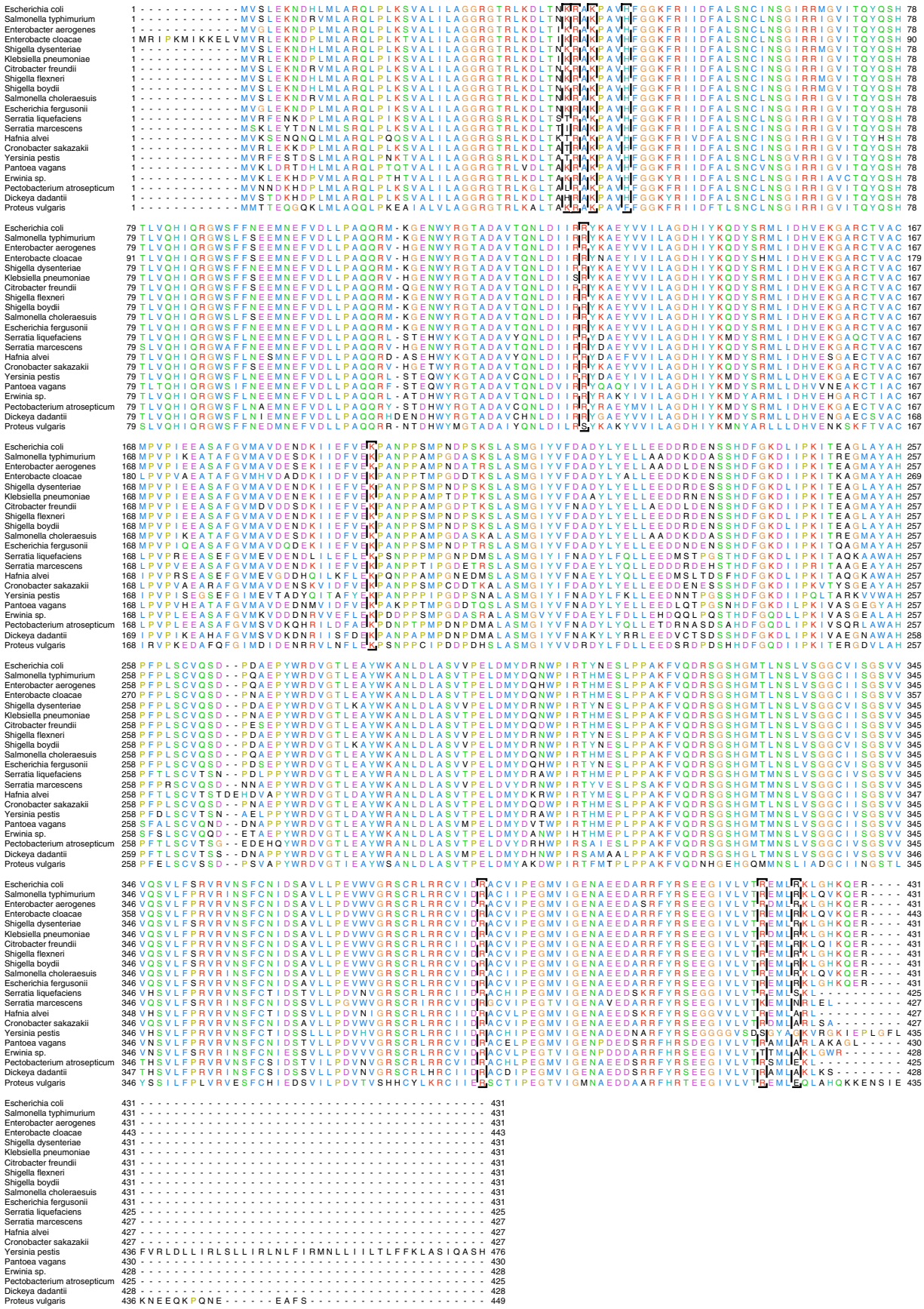

222 nm by using Hellma 110-QS quartz cuvettes with a 1-mm optical path length. Samples were 2 μM *Ec*AGPase or *Ec*AGPase mutants in 50 mM Tris-HCl, pH 8.0, 100 mM NaCl. Thermal dependences of the ellipticity were monitored in a range from 30 to 90 °C at 222 nm. Temperature was increased stepwise by 1 °C/min. Ligands effects were assessed in the same conditions for the following concentrations: AMP, 0.25 mM, 0.5 mM and 1 mM; FBP 0.5 mM and 2.5 mM. Transitions were normalized and tentatively fitted according to Equation 1 to obtain the apparent melting temperature (T_m) (67):

$$y = \frac{(yf + mf \cdot T) + (yu + mu \cdot T)e^{\left(\frac{\Delta Hm}{R}\right)\left(\frac{1}{Tm} - \frac{1}{T}\right)}}{1 + e^{\left(\frac{\Delta Hm}{R}\right)\left(\frac{1}{Tm} - \frac{1}{T}\right)}} \quad \text{(Eq. 1)}$$

where y represents the observed CD signal at 222 nm, y_f and y_u are the y axis intercepts, and m_f and m_u the slopes of the pre- and post-transition baselines, respectively, T is the temperature in K, T_m is the melting temperature, and ΔH_m is the enthalpy change of unfolding at T_m. Curve fitting was performed with KaleidaGraph 4.5.2 (Synergy Software).

EcAGPase enzymatic assay

The enzymatic activity of *Ec*AGPase and *Ec*AGPase mutants was monitored using a microplate colorimetric end-point malachite green phosphate assay (68). *Ec*AGPase catalyzes the reaction of ATP and G1P to produce ADP-Glc and PP_i (26). This reaction is coupled with an inorganic pyrophosphatase, which catalyzes the hydrolysis of PP_i to orthophosphate (P_i). P_i dosage is determined by the formation of a phosphomolybdate-malachite green complex: 1) enzymatic-coupled reactions,

$$\alpha\text{-Glucose-1P} + \text{ATP} \rightarrow \text{ADP-glucose} + P_2O_7^{4-} \quad \text{(Eq. 2)}$$

where α-glucose-1P is α-D-glucose-1-phosphate, and

$$P_2O_7^{4-} + H_2O \rightarrow 2PO_4^{3-} + 2H^+ \quad \text{(Eq. 3)}$$

2) stop reaction by complexation of Mg^{2+} with EDTA; 3) molybdate/malachite green reactions,

$$H_3PO_4 + 12\,H_2MoO_4 \rightarrow H_3PO_4(MoO_3)_{12} + 12H_2O \quad \text{(Eq. 4)}$$

and

$$H_3PMo_{12}O_{40} + HMG^{2+} \rightarrow [MG']\,(H_3PO_4(MoO_3)_{12}) + 2H^+ \quad \text{(Eq. 5)}$$

and 4) the addition of sodium citrate for reaction stabilization. Specifically, samples contained 41.1 μM (8 μg/ml) of *Ec*AGPase and 14.1 μM (1 μg/ml) pyrophosphatase (Sigma), 0.5 mM ATP, 0.5 mM G1P, 50 mM Tris-HCl pH 7.5, 2 mM $MgCl_2$, and 100 mM NaCl with or without the addition of the allosteric regulators AMP, FBP, or AMP/FBP at 0.5 mM in a final volume of 60 μl. Reactions were incubated at 20 °C and stopped at a given time by the addition of 10 μl of 50 mM EDTA, pH 8.0. Afterward, 20 μl of molybdate solution (34 mM ammonium molybdate tetrahydrate in 4N HCl; Fluka) were added to the reaction mixture and incubated at 20 °C for 3 min. Then, 60 μl of malachite green solution (1 mM malachite green oxalate salt in water; Sigma) were added to the mixture and incubated at 25 °C for 5 min. Finally, the solution was stabilized by the addition of 60 μl of sodium citrate (170 mM in water; Sigma) and measured at 620 nm in a Spectra Max M2 plate reader. Measurements were performed in quintuplicate. *Ec*AGPase and *Ec*AGPase mutants were stored in 5.1 μM (1 mg/ml) aliquots in 50 mM Tris-Cl, pH 7.5, and 100 mM NaCl at −80 °C for single use. Specific activities were stable during a period.

Overexpression of EcAGPase mutants in a glgC knock-out E. coli strain

E. coli strain K-12 carrying out a *glgC* gene deletion (*E. coli* K-12 Δ*glgC*; kanamycin-resistant strain; Keio collection; Dharmacon GE) was transformed with pTARA plasmid (chloramphenicol resistant plasmid; Addgene) to provide a controlled expression of T7 RNA polymerase. The resulting strain was subsequently transformed with pET22b-*Ec*AGPase, pET22b-*Ec*AGPase^{K39A}, pET22b-*Ec*AGPase^{R40A}, pET22b-*Ec*AGPase^{R40E}, pET22b-*Ec*AGPase^{K42A}, pET22b-*Ec*AGPase^{H46A}, pET22b-*Ec*AGPase^{R130A}, pET22b-*Ec*AGPase^{K195A}, pET22b-*Ec*AGPase^{R386A}, pET22b-*Ec*AGPase^{R419A}, or pET22b-*Ec*AGPase^{R423A} plasmid carrying the wild-type *Ec*AGPase or the corresponding mutants. *E. coli* K-12 Δ*glgC* cells transformed with pTARA and pET22b-*Ec*AGPase or the corresponding mutants were further synchronized in 10 ml of LB medium supplemented with 34 μg/ml chloramphenicol, 25 μg/ml kanamycin, and 100 μg/ml carbenicillin at 30 °C (69). After 2 passages, bacterial cultures were diluted 1:50. Aliquots of 900 μl were removed every hour and kept on ice. After 4 h, protein expression was induced by the addition of 1 mM isopropyl β-thiogalactopyranoside and 100 μg/ml arabinose. Aliquots of 900 μl were removed every hour and kept on ice for subsequent steps.

Glycogen extraction

Glycogen was extracted as previously described with minor modifications (70). Culture aliquots of 400 μl of the *E. coli* K-12 Δ*glgC* strain transformed with pTARA and pET22b-*Ec*AGPase or the corresponding mutants were centrifuged at 1200 × *g* for 10 min, and the supernatant was discarded. Pellets were resuspended in 100 μl of 8.9 M (50%) KOH and further incubated at 95 °C for 30 min. 300 μl of ice-cold 95% ethanol was added to the sample and centrifuged at 1200 × *g* for 30 min. Pellets were air-dried and stored at −20 °C.

Figure 9. Multiple sequence alignment of selected regions among members of the Enterobacteriaceae family of AGPases. Shown are *E. coli* (UniProt code P0A6V1), *Salmonella typhimurium* (UniProt code P05415); *Enterobacter aerogenes* (Genbank™ code A0A0H3FKN1); *Enterobacter cloacae* (UniProt code G8LJ14); *Shigella dysenteriae* (UniProt code E7SR47); *Klebsiella pneumoniae* (UniProt code A6TF49); *Citrobacter freundii* (Genbank™ code A0A023V613); *S. flexneri* (UniProt code P0A6V4); *S. boydii* (UniProt code Q31VJ3); *S. choleraesuis* (UniProt code Q57IU0); *E. fergusonii* (UniProt code B7LSE1); *S. liquefaciens* (Genbank™ code A0A0X8SJ44); *S. marcescens* (Genbank™ code A0A0P8VY88); *H. alvei* (Genbank™ code A0A097R790); *Cronobacter sakazakii* (UniProt code A7MGF4); *Y. pestis* (UniProt code Q1C1E1); *P. vagans* (UniProt code E1SGX9); *Erwinia* sp. (UniProt code E3DJ85); *P. atrosepticum* (UniProt code Q6CZK2); *D. dadantii* (UniProt code D2BY77); *P. vulgaris* (Genbank™ code A0A0G4Q122).

Glycogen measurement

The production of glycogen in the *E. coli* K-12 Δ*glgC* strain transformed with pTARA and pET22b-*Ec*AGPase or the corresponding mutants was determined by two colorimetric methods (71–72). Glycogen pellets were resuspended in 100 μl of water by vigorous shaking for 5 min followed by the addition of 200 μl of 10.3 mM (0.2%) anthrone (Sigma) in 95% H_2SO_4. Samples were then incubated at 95 °C for 20 min. Aliquots of 200 μl were transferred to a 96-well plate and measured at 650 nm using a Spectra Max M2 plate reader. Glucose standards were treated in a similar manner in parallel. Because anthrone is a general reagent for the detection of sugars, a second less sensitive but specific assay was used. Glycogen pellets were washed with 20 μl of saturated NH_4Cl and dry-heated at 95 °C to remove the excess ammonia. 200 μl of freshly prepared iodine reagent, a modified Lugol's iodine staining, obtained by mixing 20 μl of 102.4 mM (2.6%) I_2 and 1.6 M (26%) KI in water with 5 ml of saturated $CaCl_2$, were added. Samples were transferred to a 96-well plate and measured at 450 nm using a Spectra Max M2 plate reader. Measurements were performed in 4 and 5 replicates for the iodimetric and anthrone methods, respectively.

EcAGPase crystallization and data collection

Crystallization trials were carried out in sitting-drop 96-well plates by using a mosquito crystal robot (TTP Labtech). Crystals of *Ec*AGPase-R130A were obtained by mixing 0.25 μl of EcAGPase-R130A at 6.3 mg/ml in 50 mM Tris-HCl, pH 7.5, 100 mM NaCl with 0.25 μl of mother liquor containing 14% polyethylene glycol 3.350, 140 mM magnesium formate, 30% ethylene glycol. Crystals grew in 13 days and were directly frozen under liquid nitrogen. A complete dataset of *Ec*AGPase-R130A was collected at I04 beamline (Diamond Light Source (DLS), Didcot, Oxfordshire, UK) with an oscillation angle of 0.15° for a total of 1200 images using a Pilatus 6M-F detector. The *Ec*AGPase-R130 form crystallized in the $P2_1$ space group with 8 molecules in the asymmetric unit and diffracted to a maximum resolution of 3.09 Å (supplemental Table S1).

EcAGPase structure determination and refinement

The crystal structure of *Ec*AGPase-R130A was solved by molecular replacement with the program Phaser (73) using a tetramer from the crystal structure of *Ec*AGPase-AMP-SUC, PDB atomic coordinates 5L6V (26) as the search model. The final structure was obtained using alternate cycles of manual model-building using COOT (74) and Phenix (phenix.refine; Ref. 75) or Refmac5 (76). NCS (non-crystallographic symmetry) restraints were calculated automatically during refinement, and differences between chains were subsequently modeled. During the refinement the structure geometry was validated using Molprobity (77). The root mean square coordinates error (Å) was from a Luzzati plot (78, 79) using SFCHECK (80). Atomic coordinates and structure factors have been deposited with the Protein Data Bank, accession code 5MNI (*Ec*AGPase-R130A). Molecular graphics and structural analyses were performed with the UCSF Chimera package (81).

Enterobacterial AGPases alignment

A representative group of enterobacterial AGPase protein sequences from different species was obtained from UniProt database and sequences aligned using Clustal-Omega. Middle distance BLOSUM62 tree was performed using Jalview.

Author contributions—N. C., J. O. C., M. E. G., conceived the project. N. C., J. O. C., A. M., A. O., and A. E. performed the experiments. N. C., J. O. C., and M. E. G., analyzed the results. N. C., J. O. C., and M. E. G. wrote the manuscript.

Acknowledgments—We acknowledge Diamond Light Source (DLS) (beamline I04 and I04–1 under proposals 8302 and 10130) and the French National Synchrotron SOLEIL. Access to structural biology facilities was supported in part by the EU FP7 infrastructure grant BIOSTRUCT-X (contract 283570). We also thank all members of the Structural Glycobiology Group for valuable scientific discussions.

References

1. Ball, S., Guan, H. P., James, M., Myers, A., Keeling, P., Mouille, G., Buléon, A., Colonna, P., and Preiss, J. (1996) From glycogen to amylopectin: a model for the biogenesis of the plant starch granule. *Cell* **86,** 349–352
2. Roach, P. J., Depaoli-Roach, A. A., Hurley, T. D., and Tagliabracci, V. S. (2012) Glycogen and its metabolism: some new developments and old themes. *Biochem. J.* **441,** 763–787
3. Manners, D. J. (1991) Recent developments in our understanding of glycogen structure. *Carbohydr. Polym.* **16,** 37–82
4. Leloir, L. F., and Cardini, C. E. (1957) Biosynthesis of glycogen from uridine diphosphate glucose. *J. Am. Chem. Soc.* **79,** 6340–6341
5. Recondo, E., and Leloir, L. F. (1961) Adenosine diphosphate glucose and starch synthesis. *Biochem. Biophys. Res. Commun.* **6,** 85–88
6. Preiss, J. (1984) Bacterial glycogen synthesis and its regulation. *Annu. Rev. Microbiol.* **38,** 419–458
7. Ball, S. G., and Morell, M. K. (2003) From bacterial glycogen to starch: understanding the biogenesis of the plant starch granule. *Annu. Rev. Plant Biol.* **54,** 207–233
8. Preiss, J. (2014) Glycogen: biosynthesis and regulation. *EcoSal Plus* **6,** 1–28
9. Ballicora, M. A., Iglesias, A. A., and Preiss, J. (2003) ADP-glucose pyrophosphorylase, a regulatory enzyme for bacterial glycogen synthesis. *Microbiol. Mol. Biol. Rev.* **67,** 213–225
10. Guerin, M. E., Buschiazzo, A., Ugalde, J. E., Ugalde, R. A., and Alzari, P. M. (2003) Preliminary crystallographic studies of glycogen synthase from *Agrobacterium tumefaciens*. *Acta Crystallogr. D Biol. Crystallogr.* **59,** 526–528
11. Buschiazzo, A., Ugalde, J. E., Guerin, M. E., Shepard, W., Ugalde, R. A., and Alzari, P. M. (2004) Crystal structure of glycogen synthase: homologous enzymes catalyze glycogen synthesis and degradation. *EMBO J.* **23,** 3196–3205
12. Horcajada, C., Guinovart, J. J., Fita, I., and Ferrer, J. C. (2006) Crystal structure of an archaeal glycogen synthase: Insights into oligomerization and substrate binding of eukaryotic glycogen synthases. *J. Biol. Chem.* **281,** 2923–2931
13. Sheng, F., Jia, X., Yep, A., Preiss, J., and Geiger, J. H. (2009) The crystal structures of the open and catalytically competent closed conformation of *Escherichia coli* glycogen synthase. *J. Biol. Chem.* **284,** 17796–17807
14. Gibbons, B. J., Roach, P. J., and Hurley, T. D. (2002) Crystal structure of the autocatalytic initiator of glycogen biosynthesis, glycogenin. *J. Mol. Biol.* **319,** 463–477
15. Chaikuad, A., Froese, D. S., Berridge, G., von Delft, F., Oppermann, U., and Yue, W. W. (2011) Conformational plasticity of glycogenin and its maltosaccharide substrate during glycogen biogenesis. *Proc. Natl. Acad. Sci.* **108,** 21028–21033
16. Zeqiraj, E., Tang, X., Hunter, R. W., García-Rocha, M., Judd, A., Deak, M., von Wilamowitz-Moellendorff, A., Kurinov, I., Guinovart, J. J., Tyers, M.,

Sakamoto, K., and Sicheri, F. (2014) Structural basis for the recruitment of glycogen synthase by glycogenin. *Proc. Natl. Acad. Sci. U.S.A.* **111,** E2831–E2840
17. Ugalde, J. E., Parodi, A. J., and Ugalde, R. A. (2003) De novo synthesis of bacterial glycogen: *Agrobacterium tumefaciens* glycogen synthase is involved in glucan initiation and elongation. *Proc. Natl. Acad. Sci. U.S.A.* **100,** 10659–10663
18. Díaz, A., Martínez-Pons, C., Fita, I., Ferrer, J. C., and Guinovart, J. J. (2011) Processivity and subcellular localization of glycogen synthase depend on a non-catalytic high affinity glycogen-binding site. *J. Biol. Chem.* **286,** 18505–18514
19. Díaz, A., Díaz-Lobo, M., Grados, E., Guinovart, J. J., Fita, I., and Ferrer, J. C. (2012) Lyase activity of glycogen synthase: Is an elimination/addition mechanism a possible reaction pathway for retaining glycosyltransferases? *IUBMB Life* **64,** 649–658
20. Abad, M. C., Binderup, K., Rios-Steiner, J., Arni, R. K., Preiss, J., and Geiger, J. H. (2002) The x-ray crystallographic structure of *Escherichia coli* branching enzyme. *J. Biol. Chem.* **277,** 42164–42170
21. Feng, L., Fawaz, R., Hovde, S., Gilbert, L., Chiou, J., and Geiger, J. H. (2015) Crystal structures of *Escherichia coli* branching enzyme in complex with linear oligosaccharides. *Biochemistry* **54,** 6207–6218
22. Watson, K. A., McCleverty, C., Geremia, S., Cottaz, S., Driguez, H., and Johnson, L. N. (1999) Phosphorylase recognition and phosphorolysis of its oligosaccharide substrate: answers to a long outstanding question. *EMBO J.* **18,** 4619–4632
23. Møller, M. S., Henriksen, A., and Svensson, B. (2016) Structure and function of α-glucan debranching enzymes. *Cell. Mol. Life Sci.* **73,** 2619–2641
24. Gentner, N., and Preiss, J. (1967) Activator-inhibitor interactions in the adenosine diphosphate glucose pyrophosphorylase of *Escherichia coli* B. *Biochem. Biophys. Res. Commun.* **27,** 417–423
25. Preiss, J., Yung, S. G., and Baecker, P. A. (1983) Regulation of bacterial glycogen synthesis. *Mol. Cell. Biochem.* **57,** 61–80
26. Cifuente, J. O., Comino, N., Madariaga-Marcos, J., López-Fernández, S., García-Alija, M., Agirre, J., Albesa-Jové, D., and Guerin, M. E. (2016) Structural basis of glycogen biosynthesis regulation in bacteria. *Structure* **24,** 1613–1622
27. Blankenfeldt, W., Asuncion, M., Lam, J. S., and Naismith, J. H. (2000) The structural basis of the catalytic mechanism and regulation of glucose-1-phosphate thymidylyltransferase (RmlA). *EMBO J.* **19,** 6652–6663
28. Swift, R. V., Ong, C. D., and Amaro, R. E. (2012) Magnesium-induced nucleophile activation in the guanylyltransferase mRNA capping enzyme. *Biochemistry* **51,** 10236–10243
29. Vithani, N., Bais, V., and Prakash, B. (2014) GlmU (*N*-acetylglucosamine-1-phosphate uridyltransferase) bound to three magnesium ions and ATP at the active site. *Acta Crystallogr. F Struct. Biol. Commun.* **70,** 703–708
30. Führing, J., Cramer, J. T., Routier, F. H., Lamerz, A. C., Baruch, P., Gerardy-Schahn, R., and Fedorov, R. (2013) Catalytic mechanism and allosteric regulation of UDP-glucose pyrophosphorylase from *Leishmania major*. *ACS Catal.* **3,** 2976–2985
31. Paule, M. R., and Preiss, J. (1971) Biosynthesis of Bacterial Glycogen. X. The kinetic mechanism of adenosine diphosphoglucose pyrophosphorylase from *Rhodospirillum rubrum*. *J. Biol. Chem.* **246,** 4602–4609
32. Kornberg, A. (1962) On the metabolic significance of phosphorolytic and pyrophosphorolytic reactions. in *Horizons in Biochemistry* (Kasha, H., and Pullman, P., eds) pp. 251–264, Academic Press, New York, NY
33. Lahti, R. (1983) Microbial inorganic pyrophosphatases. *Microbiol. Rev.* **47,** 169–178
34. Preiss, J. (1978) Regulation of adenosine diphosphate glucose pyrophosphorylase. *Adv. Enzymol. Relat. Areas Mol. Biol.* **46,** 317–381
35. Meyer, C. R., Yirsa, J., Gott, B., and Preiss, J. (1998) A kinetic study of site-directed mutants of *Escherichia coli* ADP-glucose pyrophosphorylase: the role of residue 295 in allosteric regulation. *Arch. Biochem. Biophys.* **352,** 247–254
36. Ball, S., Colleoni, C., Cenci, U., Raj, J. N., and Tirtiaux, C. (2011) The evolution of glycogen and starch metabolism in eukaryotes gives molecular clues to understand the establishment of plastid endosymbiosis. *J. Exp. Bot.* **62,** 1775–1801
37. Ugalde, J. E., Lepek, V., Uttaro, A., Estrella, J., Iglesias, A., and Ugalde, R. A. (1998) Gene organization and transcription analysis of the *Agrobacterium tumefaciens* glycogen (glg) operon: two transcripts for the single phosphoglucomutase gene. *J. Bacteriol.* **180,** 6557–6564
38. Preiss, J., and Romeo, T. (1989) Physiology, biochemistry, and genetics of bacterial glycogen synthesis. *Adv Microb Physiol* **30,** 183–238
39. Cupp-Vickery, J. R., Igarashi, R. Y., Perez, M., Poland, M., and Meyer, C. R. (2008) Structural analysis of ADP-glucose pyrophosphorylase from the bacterium *Agrobacterium tumefaciens*. *Biochemistry* **47,** 4439–4451
40. Albesa-Jové, D., and Guerin, M. E. (2016) The conformational plasticity of glycosyltransferases. *Curr. Opin. Struct. Biol.* **40,** 23–32
41. Albesa-Jové, D., Giganti, D., Jackson, M., Alzari, P. M., and Guerin, M. E. (2014) Structure-function relationships of membrane-associated GT-B glycosyltransferases. *Glycobiology* **24,** 108–124
42. Bejar, C. M., Ballicora, M. A., Gómez-Casati, D. F., Iglesias, A. A., and Preiss, J. (2004) The ADP-glucose pyrophosphorylase from *Escherichia coli* comprises two tightly bound distinct domains. *FEBS Lett.* **573,** 99–104
43. Perutz, M. F. (1989) Mechanisms of cooperativity and allosteric regulation in proteins. *Q. Rev. Biophys.* **22,** 139–237
44. Gardiol, A., and Preiss, J. (1990) *Escherichia coli* E-39 ADP glucose synthetase has different activation kinetics from the wild-type allosteric enzyme. *Arch. Biochem. Biophys.* **280,** 175–180
45. Figueroa, C. M., Esper, M. C., Bertolo, A., Demonte, A. M., Aleanzi, M., Iglesias, A. A., and Ballicora, M. A. (2011) Understanding the allosteric trigger for the fructose 1,6-bisphosphate regulation of the ADP-glucose pyrophosphorylase from *Escherichia coli*. *Biochimie* **93,** 1816–1823
46. Jin, X., Ballicora, M. A., Preiss, J., and Geiger, J. H. (2005) Crystal structure of potato tuber ADP-glucose pyrophosphorylase. *EMBO J.* **24,** 694–704
47. Preiss, J., Shen, L., and Partridge, M. (1965) The activation of *Escherichia coli* ADP-glucose pyrophosphorylase. *Biochem. Biophys. Res. Commun.* **18,** 180–185
48. Ribéreau-Gayon, G., Sabraw, A., Lammel, C., and Preiss, J. (1971) Biosynthesis of bacterial glycogen IX: regulatory properties of the adenosine diphosphate glucose pyrophosphorylases of the Enterobactericeae. *Arch. Biochem. Biophys.* **142,** 675–692
49. Hill, M. A., Kaufmann, K., Otero, J., and Preiss, J. (1991) Biosynthesis of bacterial glycogen: mutagenesis of a catalytic site residue of ADP-glucose pyrophosphorylase from *Escherichia coli*. *J. Biol. Chem.* **266,** 12455–12460
50. Ballicora, M. A., Dubay, J. R., Devillers, C. H., and Preiss, J. (2005) Resurrecting the ancestral enzymatic role of a modulatory subunit. *J. Biol. Chem.* **280,** 10189–10195
51. Frueauf, J. B., Ballicora, M. A., and Preiss, J. (2001) Aspartate residue 142 is important for catalysis by ADP-glucose pyrophosphorylase from *Escherichia coli*. *J. Biol. Chem.* **276,** 46319–46325
52. Bejar, C. M., Jin, X., Ballicora, M. A., and Preiss, J. (2006) Molecular architecture of the glucose 1-phosphate site in ADP-glucose pyrophosphorylases. *J. Biol. Chem.* **281,** 40473–40484
53. Steitz, T. A., Smerdon, S. J., Jäger, J., and Joyce, C. M. (1994) A unified polymerase mechanism for nonhomologous DNA and RNA polymerases. *Science* **266,** 2022–2025
54. Ballicora, M. A., Sesma, J. I., Iglesias, A. A., and Preiss, J. (2002) Characterization of chimeric ADPglucose pyrophosphorylases of *Escherichia coli* and *Agrobacterium tumefaciens*: importance of the C terminus on the selectivity for allosteric regulators. *Biochemistry* **41,** 9431–9437
55. Wattam, A. R., Abraham, D., Dalay, O., Disz, T. L., Driscoll, T., Gabbard, J. L., Gillespie, J. J., Gough, R., Hix, D., Kenyon, R., Machi, D., Mao, C., Nordberg, E. K., Olson, R., Overbeek, R., Pusch, G. D., *et al.* (2014) PATRIC, the bacterial bioinformatics database and analysis resource. *Nucleic Acids Res.* **42,** D581–D591
56. Monod, J., Changeaux, J. P., and Jacob, F. (1963) Allosteric proteins and cellular control systems. *J. Mol. Biol.* **6,** 306–329
57. Fushinobu, S., Kamata, K., Iwata, S., Sakai, H., Ohta, T., and Matsuzawa, H. (1996) Allosteric activation of L-lactate dehydrogenase analyzed by hybrid enzymes with effector-sensitive and -insensitive subunits. *J. Biol. Chem.* **271,** 25611–25616

58. Ormö, M., Bystrom, C. E., and Remington, S. J. (1998) Crystal structure of a complex of *Escherichia coli* glycerol kinase and an allosteric effector fructose 1,6-bisphosphate. *Biochemistry* **37,** 16565–16572
59. Valentini, G., Chiarelli, L., Fortin, R., Speranza, M. L., Galizzi, A., and Mattevi, A. (2000) The allosteric regulation of pyruvate kinase. *J. Biol. Chem.* **275,** 18145–18152
60. Monod, J., Wyman, J., and Changeux, J. P. (1965) On the nature of allosteric transitions: a plausible model. *J. Mol. Biol.* **12,** 88–118
61. Jurica, M. S., Mesecar, A., Heath, P. J., Shi, W., Nowak, T., and Stoddard, B. L. (1998) The allosteric regulation of pyruvate kinase by fructose 1,6-bisphosphate. *Structure* **6,** 195–210
62. Ikehara, Y., Arai, K., Furukawa, N., Ohno, T., Miyake, T., Fushinobu, S., Nakajima, M., Miyanaga, A., and Taguchi, H. (2014) The core of allosteric motion in *Thermus caldophilus* L-lactate dehydrogenase. *J. Biol. Chem.* **289,** 31550–31564
63. Clarke, A. R., Wigley, D. B., Barstow, D. A., Chia, W. N., Atkinson, T., and Holbrook, J. J. (1987) A single amino acid substitution deregulates a bacterial lactate dehydrogenase and stabilizes its tetrameric structure. *Biochim. Biophys. Acta* **913,** 72–80
64. Sweetlove, L. J., Burrell, M. M., and ap Rees, T. (1996) Starch metabolism in tubers of transgenic potato (*Solanum tuberosum*) with increased ADP-glucose pyrophosphorylase. *Biochem. J.* **320,** 493–498
65. Stark, D. M., Timmerman, K. P., Barry, G. F., Preiss, J., and Kishore, G. M. (1992) Regulation of the amount of starch in plant tissues by ADP glucose pyrophosphorylase. *Science* **258,** 287–292
66. Tuncel, A., and Okita, T. W. (2013) Improving starch yield in cereals by overexpression of ADP glucose pyrophosphorylase: expectations and unanticipated outcomes. *Plant Sci.* **211,** 52–60
67. Sotomayor-Pérez, A. C., Subrini, O., Hessel, A., Ladant, D., and Chenal, A. (2013) Molecular crowding stabilizes both the intrinsically disordered calcium-free state and the folded calcium-bound state of a repeat in toxin (RTX) protein. *J. Am. Chem. Soc.* **135,** 11929–11934
68. Fusari, C., Demonte, A. M., Figueroa, C. M., Aleanzi, M., and Iglesias, A. A. (2006) A colorimetric method for the assay of ADP-glucose pyrophosphorylase. *Anal. Biochem.* **352,** 145–147
69. Wouter, A., Duetz, M. C., and Bills, G. (2010) Chapter 8: Miniaturization of fermentations, in *Manual of Industrial Microbiology and Biotechnology* (Lynd, L. R., Zhao, H., Katz, L., Baltz, R. H., Bull, A. T., Junker, B., Masurekar, P., Davies, J. E., Reeves, C. D., and Demain, A. L., eds) 3rd Ed., pp. 99–116, American Society for Microbiology, Washington, D. C.
70. Preiss, J., Greenberg, E., and Sabraw, A. (1975) Biosynthesis of bacterial glycogen. Kinetic studies of a glucose-1-phosphate adenylyltransferase (EC 2.7.7.27) from a glycogen-deficient mutant of *Escherichia coli* B. *J. Biol. Chem.* **250,** 7631–7638
71. Krisman, C. R. (1962) A method for the calorimetric estimation of glycogen with iodine. *Anal. Biochem.* **4,** 17–23
72. Archibald, A. R., Fleming, I. D., Liddle, A. M., Manners, D. J., Mercer, G. A., and Wright, A. (1961) α-1,4-Glucosans. Part XI. The absorption spectra of glycogen- and amylopectin-iodine complexes. *J. Chem. Soc.* **232,** 1183–1190
73. McCoy, A. J., Grosse-Kunstleve, R. W., Adams, P. D., Winn, M. D., Storoni, L. C., and Read, R. J. (2007) Phaser crystallographic software. *J. Appl. Crystallogr.* **40,** 658–674
74. Emsley, P., Lohkamp, B., Scott, W. G., and Cowtan, K. (2010) Features and development of Coot. *Acta Crystallogr. D Biol. Crystallogr.* **66,** 486–501
75. Adams, P. D., Afonine, P. V., Bunkóczi, G., Chen, V. B., Davis, I. W., Echols, N., Headd, J. J., Hung, L. W., Kapral, G. J., Grosse-Kunstleve, R. W., McCoy, A. J., Moriarty, N. W., Oeffner, R., Read, R. J., Richardson, D. C., *et al.* (2010) PHENIX: A comprehensive Python-based system for macromolecular structure solution. *Acta Crystallogr. D Biol. Crystallogr.* **66,** 213–221
76. Murshudov, G. N., Skubák, P., Lebedev, A. A., Pannu, N. S., Steiner, R. A., Nicholls, R. A., Winn, M. D., Long, F., and Vagin, A. A. (2011) REFMAC5 for the refinement of macromolecular crystal structures. *Acta Crystallogr. D Biol. Crystallogr.* **67,** 355–367
77. Chen, V. B., Arendall, W. B., 3rd, Headd, J. J., Keedy, D. A., Immormino, R. M., Kapral, G. J., Murray, L. W., Richardson, J. S., and Richardson, D. C. (2010) MolProbity: All-atom structure validation for macromolecular crystallography. *Acta Crystallogr. D Biol. Crystallogr.* **66,** 12–21
78. Luzzati, V. (1952) Traitement statistique des erreurs dans la determination des structures cristallines. *Acta Cryst.* **5,** 802–810
79. Vaguine, A. A., Richelle, J., and Wodak, S. J. (1999) SFCHECK: a unified set of procedure for evaluating the quality of macromolecular structure-factor data and their agreement with atomic model. *Acta Crystallogr. D Biol. Crystallogr.* **55,** 191–205
80. Laskowski, R. A. (2003) Structural quality assurance. *Methods Biochem. Anal.* **44,** 273–303
81. Pettersen, E. F., Goddard, T. D., Huang, C. C., Couch, G. S., Greenblatt, D. M., Meng, E. C., and Ferrin, T. E. (2004) UCSF chimera: a visualization system for exploratory research and analysis. *J. Comput. Chem.* **25,** 1605–1612
82. Lodeiro, A. R., di Lorenzo, O., Petruccelli, S., Molina-Ortiz, S., and Sorgentini, D. (1994) An experiment on glycogen biosynthesis in *Escherichia coli*. *Biochem. Educ.* **22,** 213–215